

Can giant radio halos probe the merging rate of galaxy clusters?

R. Cassano¹, G. Brunetti¹, C. Giocoli², and S. Ettori^{3,4}

¹ INAF-Istituto di Radioastronomia, via P. Gobetti, 101, 40129, Bologna, Italy
e-mail: rcassano@ira.inaf.it

² Aix Marseille Université, CNRS, LAM (Laboratoire d'Astrophysique de Marseille) UMR 7326, 13388, Marseille, France

³ INAF/Osservatorio Astronomico di Bologna, via Ranzani 1, I-40127 Bologna, Italy

⁴ INFN, Sezione di Bologna, viale Berti Pichat 6/2, I-40127 Bologna, Italy

June 24, 2016

ABSTRACT

Observations of galaxy clusters both in the radio and X-ray bands probe a direct link between cluster mergers and giant radio halos, suggesting that these sources can be used as probes of the cluster merging rate with cosmic time. However, while all giant radio halos are found in merging clusters not every merging cluster host a giant radio halo. In this paper we carry out an *explorative* study that combines the observed fractions of merging clusters and radio halos with the merging rate predicted by cosmological simulations and attempt to infer constraints on merger properties of clusters that appear disturbed in X-rays and of clusters that host radio halos. We use classical morphological parameters to identify merging systems and analyze the currently largest (mass-selected $M_{500} \gtrsim 6 \times 10^{14} M_{\odot}$ and $0.2 \leq z \leq 0.33$) sample of galaxy clusters with radio and X-ray data; we extract this sample from the Planck Sunyaev-Zeldovich cluster catalogue. We found that the fraction of merging clusters in this sample is $f_m \sim 62 - 67\%$ while that of clusters with radio halos is $f_{RH} \sim 44 - 51\%$. We assume that the morphological disturbance measured in the X-rays is driven by the merger with the largest mass ratio, ξ ($\xi = M_i/M_1 < 1$ with M_i and M_1 being the progenitor masses), that is still ongoing in the cluster at the epoch of observation. Results from theoretical studies allow to derive the fraction of mergers with mass ratio above a minimum threshold (those with $\xi \gtrsim \xi_{min}$) in our sample, under the assumption of a timescale τ_m for the duration of merger-induced disturbance. The comparison of the theoretical merger fraction with the observed one allows to constrain a region in the (ξ_{min}, τ_m) plane. We find that under the assumption of $\tau_m \sim 2 - 3$ Gyr, as constrained by simulations, the observed merger fraction matches the theoretical one for $\xi_{min} \sim 0.1 - 0.18$. This is consistent with optical and near-IR observations of galaxy clusters in the sample that constrain $\xi_{min} \simeq 0.14 - 0.16$ through weak lensing analysis or study of the velocity distribution of galaxies in the clusters. The fact that radio halos are found only in a fraction of merging galaxy clusters may suggest that merger events generating radio halos are characterized by larger mass ratio; this seems supported by optical/near-IR observations of RH clusters in the sample that indeed allow to constrain $\xi_{min} \sim 0.2 - 0.25$. Alternatively, radio halos may be generated in all mergers but their lifetime is shorter (by $\sim f_{RH}/f_m$) than the timescale of the merger-induced disturbance. We stress that this is an *explorative* study, however it suggests that follow up studies using the forthcoming radio surveys and adequate numerical simulations have the potential to derive quantitative constraints on the link between cluster merging rate and radio halos at different cosmic epochs and for different cluster masses.

Key words. Galaxies: clusters: intracluster medium – Cosmology: theory – Radio continuum: general - X-rays: galaxies: clusters

1. Introduction

In the paradigm of the hierarchical structure formation scenario, galaxy clusters, the largest and more recently assembled structures in the Universe, form via mergers of smaller halos and continuous accretion of unbound matter. The process of mass accretion of dark-matter halos is a clear outcome of the cosmological model. It can be statistically investigated with N-body simulations and semi-analytical models through the identification of merger trees of dark matter halos, which lead to the derivation of the mass accretion history and merging rate as a function of redshift, halo mass and mass ratio of the progenitors (e.g., van den Bosch 2002; Giocoli et al. 2007; Moreno et al. 2008; Fakhouri & Ma 2008; McBride et al. 2009; Fakhouri et al. 2010; Giocoli et al. 2012).

Observationally, the exploration of the merging rate of dark matter haloes has only been attempted on the scales of galaxies by using two main methods for tracing the merging history in the observations: morphological identification techniques (Conselice et al. 2003; Lotz, Primack & Madau 2004) and the close galaxy pair method (e.g., Patton et al. 2000; De Propriis et al.

2005). These methods are then combined with the merger timescale derived from N-body simulations to get the merging rate (e.g., Lotz et al. 2011; Jian et al. 2012; Conselice 2014). However, current results are inconclusive, because the merger rate of dark-matter halos and the merger rate of galaxies do not necessarily coincide because they are related by dissipative processes (dynamical friction, tidal interaction, stellar feedback, etc.) that are difficult to model (Fakhouri & Ma 2008; Guo & White 2008; Lotz et al. 2011; Hopkins et al. 2013). Dissipative processes are instead less relevant during the mass accretion of galaxy clusters. Nevertheless only recently a method based on the possibility to measure the cluster mass in a thin spherical shell surrounding the cluster beyond R_{200} (with the caustic technique) and by estimating its infalling time (e.g., Diaferio 2015; De Boni et al. 2016), have been proposed to measure the mass accretion rate of galaxy clusters. However, in general, the growth of structures on the scale of galaxy clusters remains poorly explored from an observational perspective (e.g., Lemze et al. 2013).

Mergers between clusters are the most energetic phenomena since the big-bang, with a release of a gravitational potential energy of $\sim 10^{63} - 10^{64}$ ergs during one cluster crossing time

(~ 1 Gyr). During such events shock waves and random vortical flows, if not turbulence, are produced in the intracluster medium (ICM) (e.g., Kulsrud et al. 1997; Norman & Bryan 1999; Ricker & Sarazin 2001). These motions originate due to vorticity generation in oblique accretion shocks and instabilities during the cluster formation, and in the wakes of the smaller subclusters (e.g., Subramanian et al. 2006; Brunetti & Jones 2014; Brüggen & Vazza 2015). The bulk of the gravitational energy associated with the collision will be released as thermal energy in the final system (e.g., Kravtsov & Borgani 2012), while another fraction can be channeled into non-thermal plasma components, *i.e.*, relativistic particles and magnetic fields in the ICM (e.g., Brunetti & Jones 2014). The existence of cosmic ray electrons and magnetic fields in the ICM is in fact demonstrated by radio observations. Cluster-scale (\sim Mpc-scale) diffuse synchrotron emission is frequently found in merging galaxy clusters in the form of so-called giant radio halos (hereafter RH), apparently unpolarized synchrotron emission associated with the cluster X-ray emitting regions, and giant radio relics, elongated and often highly polarized synchrotron sources typically seen in the clusters outskirts (e.g., Feretti et al. 2012, for an observational review). The properties of radio relics suggest a connection with large scale shocks that cross the ICM during mergers and that may accelerate locally injected electrons or reaccelerate pre-existing energetic electrons, while RH likely trace gigantic turbulent regions in the ICM, where relativistic electrons can be reaccelerated through scattering with MHD turbulence (e.g., Brunetti & Lazarian 2007; Brüggen et al. 2012).

In the last decades, radio observations of statistical samples of galaxy clusters have shown that RHs are not ubiquitous, only $\sim 20 - 30\%$ of the X-ray luminous ($L_X(0.1 - 2.4 \text{ keV}) \geq 5 \times 10^{44} \text{ erg/s}$) clusters host a RH (e.g., Venturi et al. 2008; Kale et al. 2015), while the fraction of clusters with RH becomes larger in SZ-selected clusters (e.g., Basu 2012; Cassano et al. 2013; Sommer & Basu 2014; Cuciti et al. 2015). Most important, it was found that RH and non-RH clusters are clearly separated in the $P_{1.4} - L_X$ and $P_{1.4} - M_{500}$ (Y_{500}) diagrams according to the cluster dynamical status, with RH always associated to dynamically disturbed clusters and clusters without RHs statistically more “relaxed” (e.g., Brunetti et al. 2007, 2009; Cassano et al. 2010, 2013). The connection between RHs and merging clusters has been further supported by a number of independent studies (e.g., Rossetti et al. 2011; Wen & Han 2015; Parekh et al. 2015; Mantz et al. 2015; Yuan et al. 2015; Kale & Parekh 2016). The RH-cluster merger connection suggests that RHs can be used as signposts of cluster mergers and support the idea that RH are “transient” phenomena tracing turbulent region in the ICM during the process of cluster formation. However not all merging clusters host a giant RH (see Cassano et al. 2013 and ref. therein) and this poses fundamental questions about the conditions that are necessary to generate cluster-scale synchrotron diffuse emission.

Interestingly the connection between mergers and non-thermal phenomena also opens to the possibility to infer constraints on the cluster merging rate from radio observations. In this paper we start exploring this possibility. In particular we attempt to combine the observed fraction of merging clusters and the observed fraction of RH in clusters with the merging rate predicted by cosmological simulations to infer constraints on the properties of the mergers that induce disturbances observed in the X-rays and of those responsible for RH.

We stress that this is an explorative study, with the main aim to start to investigate the possibility to use diffuse radio emission in galaxy clusters as tracer of the cluster dynamical status. In par-

ticular, we stress that current statistical information is still limited to very massive ($M_{500} \gtrsim 6 \times 10^{14} M_\odot$) and relatively nearby systems ($z \simeq 0.2 - 0.33$), while we anticipate that better constraints can be obtained using less massive systems or clusters at higher redshifts.

In Sect.2 we present the cluster sample and derive the fractions of merging clusters and that of clusters with RH; in Sect.3 we describe the formalism by Fakhouri, Ma & Boylan-Kolchin (2010) to derive the merging rate in simulations and derive the expected merger fraction. In Sect.4 we compare the observed merger fraction and RH fraction with expectations from simulations and attempt to constrain the properties that cluster mergers should have to explain the observed fraction of clusters with X-ray disturbances and that of clusters with RH. Finally, in Sect.5 we summarize the main results and discuss the main implications for the origin of giant RH in galaxy clusters.

A Λ CDM cosmology ($H_0 = 70 \text{ km s}^{-1} \text{ Mpc}^{-1}$, $\Omega_m = 0.3$, $\Omega_\Lambda = 0.7$) is adopted.

2. Data and sample selection

We used the Planck Sunyaev-Zeldovich (SZ) cluster catalogue (PSZ, Planck Collaboration XXIX 2014a) to select 54 clusters with $M_{500} \gtrsim 6 \times 10^{14} M_\odot$ ¹, redshift $0.2 \leq z \leq 0.33$ and $\delta > -30^\circ$ and $|b| \geq \pm 20^\circ$, where b is the galactic latitude (Tab. A.1). With such a selection the sample has a mass-completeness of $\sim 80\%$ ².

This selection has been thought to optimize the available information in the radio band, indeed 37 out of 54 clusters belong to the Giant Metrewave Radio Telescope (GMRT) RH Survey and its extension (EGRHS; Venturi et al. 2007, 2008; Kale et al. 2013, 2015) and for 39 out of 54 clusters ($\sim 72\%$ of the sample) information about the presence/absence of diffuse radio emission is available. In particular, 17 clusters host giant RH, while 3 clusters host candidate RHs (see Tab. A.1). The fraction of RH, defined as $f_{RH} = N_H/N_{tot}$, with N_H being the number of RH and N_{tot} the total number of clusters, is thus $\sim 44\%$ and can reach $\sim 51\%$ if we include the 3 uncertain cases.

51 out of 54 clusters ($\sim 94\%$ of the sample, including all the 39 clusters with available radio information) have X-ray data (Chandra and/or XMM-Newton) that can be used to derive information about the cluster dynamical status. In particular, 41 of these clusters have Chandra data for which morphological indicators, such as the power ratio P_3/P_0 (e.g., Buote & Tsai 1995), the emission centroid shift w (e.g., Mohr et al. 1993) and the surface brightness concentration parameter c (e.g., Santos et al. 2008) can be homogeneously derived to quantitatively establish the cluster dynamical status. Following Cassano et al. (2010, 2013), we adopted an algorithm for an automatic detection of the point sources, which are then removed from the images. We study the cluster substructures on a typical RH scale analyzing the surface brightness inside an aperture radius of 500 kpc, since we are interested in the cluster dynamics on the scales where the energy is most likely dissipated to generate the radio emission. We briefly remind that the power ratio is a multipole decomposition of the two-dimensional projected mass distribution within a given aperture, and P_3/P_0 is the lowest power ratio moment providing a clear substructure measure (Böhringer et al. 2010). The

¹ The values of M_{500} in the PSZ catalogue are obtained from Y_{500} as described in Sect.7.2.2 in Planck Collaboration XXIX 2014a.

² This completeness is estimated in Y_{SZ} by Planck Collaboration (2014a) and then converted in “mass completeness” using scaling relations in Planck Collaboration XX (2014b; see Fig.28 in Planck Collaboration 2014a).

centroid shift w is defined as the standard deviation of the projected separation between the peak and the centroid of the cluster X-ray brightness distribution in unit of the aperture radius. The concentration parameter c is defined as the ratio of the peak (within 100 kpc) over the ambient (within 500 kpc) X-ray surface brightness. Following previous papers (Cassano et al. 2010, 2013; Cuciti et al. 2015), we adopt the following threshold values to classify clusters as mergers: $P_3/P_0 \gtrsim 1.2 \times 10^{-7}$, $w \gtrsim 0.012$ and $c \lesssim 0.2$. For 32 clusters with Chandra data morphological parameters are already published in Cassano et al. (2010, 2013) and Cuciti et al. (2015), here we derive the morphological quantities for additional 9 clusters following the approach outlined above (and described in previous works; see *e.g.*, Sect. 3 of Cassano et al. 2010 for details). The resulting dynamical status of the clusters, “merger” vs “relaxed”, is reported in Tab. A.1 (column 6); the values of the morphological parameters for the 41 clusters with Chandra data are reported in Tab.A.2.

10 more clusters with available XMM-Newton observations can be added to this sample and after a visual inspection of their images we can assess (even if with less confidence) their dynamical status (also reported in Tab. A.1, column 6).

In deriving the merger fraction³ we assume that the disturbance we measure in the X-rays is mainly due to the merger with the largest mass ratio that is ongoing in the system at the epoch of the observation, *i.e.*, a binary merger approximation. Under this assumption the merger fraction is equivalent to the fraction of clusters that is actually in phase of merger (where with clusters we refer to the final product of the merger). Considering the sample of 39 clusters with available radio information, we found that the fraction of dynamically disturbed systems, or the merger fraction, defined as $f_m = N_m/N_{tot}$ with N_m being the number of merging clusters, is $\sim 62 - 67\%$ (including the uncertainty on the classification of two clusters; see Tab. A.1). If we extend this analysis to the sample of 51 clusters with X-ray data, we found $f_m \sim 65 - 69\%$. We can only speculate on the fraction of RH in this latter sample, for instance, by assuming that the fraction of merging clusters with RH in these additional 12 clusters is the same that we measure in the sample of 39 clusters (that is $\sim 70\%$), we obtain $f_H \sim 45 - 51\%$. The derived fractions are summarized in Tab.1.

Table 1. Cluster’s fractions

cluster sample	f_m	f_{RH}
39 clusters	62-67%	44-51%
51 clusters	65-69%	45-51%

Calculations in the paper will be based on the fractions extracted from the sample of 39 clusters (for which both radio and X-ray data⁴ are available), although these fractions are not expected to change significantly in the extended sample (under reliable assumptions, see Tab. 1).

³ To compare the observed merger fraction with theoretical expectations we convert the M_{500} to virial masses, M_{vir} , by assuming a NFW profile (*e.g.*, Navarro, Frenk & White 1997) for the dark matter halos and the concentration-mass relation in Duffy et al. (2008), see Appendix A in Ettori et al. (2010). Both the values of M_{500} and M_{vir} are reported in Tab. A.1.

⁴ Note that for 4 out of 39 clusters the dynamical classification is based on a visual inspection of the XMM-Newton cluster image.

3. Merging rate of halos from simulations

In the Lambda cold dark matter (Λ CDM) scenario dark matter halos grow in mass and size primarily through mergers with other halos: merger with comparable mass halos (“major mergers”), merger with smaller satellite halos (“minor mergers”). To derive the merging rate of halos we use the result derived from the combined Millennium (Springel et al. 2005) and Millennium-II (Boylan-Kolchin et al. 2009) simulations (Fakhouri, Ma & Boylan-Kolchin 2010; FMB10 hereafter). FMB10 used merger trees of dark matter halos to extract a catalog of mergers containing for each descendant halo at redshift $z_d \geq 0$ with mass M the N_p ($N_p \geq 1$) progenitors at $z_p = z_d + \Delta z$, with masses $M_1 \geq M_2 \geq \dots M_{N_p}$. To derive the merging rate they include *all* the progenitors (above a given mass threshold), and since they do not have information about the order the progenitors merge, they assume that each progenitor M_i with $i \geq 2$ mergers with the most massive progenitor M_1 at a given point between z_p and z_d . Thus a descendant halo with N_p progenitors is assumed to be the result of $N_p - 1$ binary merger events with mass ratio $\xi = M_i/M_1 \leq 1$ ($i = 2, \dots, N_p$). The progenitor mass ratio, ξ , is defined so that, for instance, $\xi = 0.3$ indicates major mergers (with mass ratio 1 : 3), while $\xi = 0.1$ indicates mergers with mass ratio 1 : 10. The derived mean merging rate per halo, $dN_m/d\xi/dz$, that gives the mean number of mergers per unit halo per unit z per unit ξ , can be well described by the following formula (FMB10):

$$\frac{dN_m}{d\xi dz}(M, \xi, z) = A \left(\frac{M}{10^{12} M_\odot} \right)^\alpha \xi^\beta \exp \left[\left(\frac{\xi}{\tilde{\xi}} \right)^\gamma \right] (1+z)^\eta, \quad (1)$$

were the best-fit parameters are: $\alpha = 0.133$, $\beta = -1.995$, $\gamma = 0.263$, $\eta = 0.0993$ and $A = 0.0104$, $\tilde{\xi} = 9.72 \times 10^{-3}$. This formula has a negligible dependence on the redshift and it is also nearly independent of the mass. The main dependence is on the mass ratio ξ , so that the number of merger per halo is larger for smaller mass ratio. For example, the number of mergers (per halo) with $\xi = 0.01$ is about 90 times larger than the number of mergers with $\xi = 0.1$ (see Fig.1, right panel, in FMB10).

Integrating Eq. 1 for $\xi \geq \xi_{min}$ and between z_0 and z one obtains the cumulative number of mergers, $N_m(\xi_{min}, M_0, z_0, z)$, that is the total number of mergers with $\xi \geq \xi_{min}$ that a halo of mass M_0 at redshift z_0 has encountered between z_0 and an earlier z during the halo’s history:

$$N_m(\xi_{min}, M_0, z_0, z) = \int_{z_0}^z dz \int_{\xi_{min}}^1 d\xi \frac{dN_m}{d\xi dz}(M(z), \xi, z), \quad (2)$$

where $M(z)$ is the mass accretion history and can be obtained integrating the fitting formula for the mass accretion rate, $\dot{M} = (M_0 - M_1)/\Delta t$ (where M_0 is the descendant mass at time t and M_1 is the mass of its most massive progenitor at time $t - \Delta t$), that is given by (FMB10):

$$\langle \dot{M} \rangle_{mean} = 46.1 M_\odot \text{yr}^{-1} \left(\frac{M}{10^{12} M_\odot} \right)^{1.1} \times E_z (1 + 1.11 z), \quad (3)$$

The quantity we derived observationally is the merger fraction, that is the fraction of clusters with significant dynamical disturbance in the X-rays (see Sect. 2). To compare this quantity with expectations given by Eqs. (1)–(3), we need to assume a merger timescale, τ_m , associated with the duration of

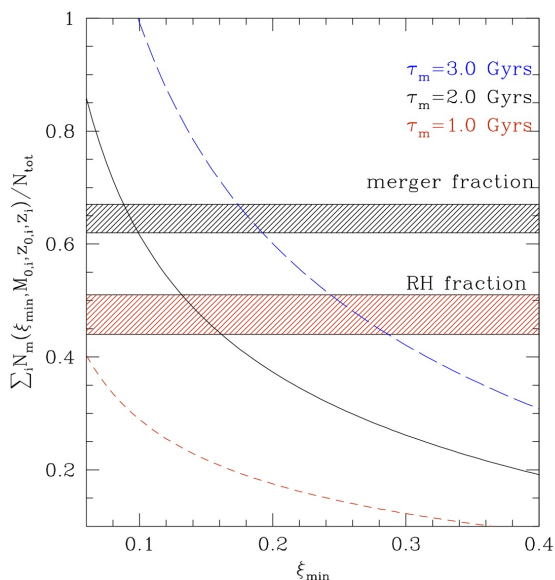


Fig. 1. Predicted average merger fraction for clusters in the sample as a function of ξ_{\min} , assuming three different values for the merger timescale $\tau_m = 1, 2, 3$ Gyr (from bottom to top). The observed merger fraction and RH fraction are also reported (shadowed regions).

the morphological disturbance that we infer from X-ray images. This is a free parameter in our calculations that however can be constrained through numerical simulations (see Sect. 4). We derive the average fraction of mergers with $\xi \geq \xi_{\min}$ expected in our sample by integrating Eq. 2 for each cluster of the sample with mass M_0 and redshift z_0 up to the redshift z corresponding to the look back time τ_m and then computing $\sum_i N_m(\xi_{\min}, M_{0,i}, z_{0,i}, z_i) / N_{\text{tot}}$, where the sum is on the N_{tot} number of clusters in the sample. The derived average merger fraction is reported in Fig. 1 as a function of ξ_{\min} for three values of τ_m ($\tau_m = 1, 2, 3$ Gyr) and is compared with the observed merger fraction and the observed fraction of clusters with RH (shadowed regions).

The predicted merger fraction decreases for larger mass ratios simply because major mergers are less common than minor ones, and it obviously increases by assuming larger timescales.

4. Comparison with theory

The comparison between the “observed” and “theoretical” merging fractions allows to derive constraints on relevant parameters, such as τ_m and ξ_{\min} . Before proceeding in this direction, we need to discuss some caveats in our procedures. In principle, the comparison between the “observed” and “theoretical” merging fractions allows to derive constraints on relevant parameters, such as τ_m and ξ_{\min} .

4.1. Caveats

The observed merger fraction is derived by measuring the fraction of clusters with significant X-ray disturbances. This means that our method is limited to events with significant mass accretion, otherwise it would be difficult to classify these events as “mergers” based on the morphological parameters. The dynamical parameters are derived within a region of radius 500 kpc. On the other hand, in FMB10 the merger fraction is derived from the merging rate which considers all the infalling halos within the

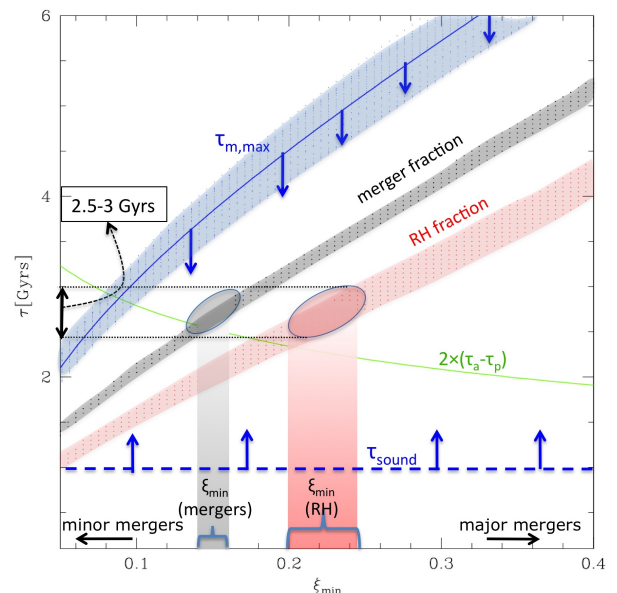


Fig. 2. Allowed regions of parameters (ξ_{\min} , τ_m) constrained by requiring that the observed merger fraction (black region) and RH fraction (red regions) match those predicted by theory (these regions account for the uncertainty in the observed fraction). For each ξ_{\min} the maximum allowed value of τ_m , $\tau_{m,\max}$ (blue region with arrows; see Sect. 4.2) and a lower limit to τ_m (horizontal blue dashed line, see Sect. 4.2) are also shown. The merger-timescale constrained by cosmological simulation is also reported (green line; Tormen et al. 2004). Ranges of ξ_{\min} constrained through optical/near-IR observations of galaxy clusters in the sample (see Sect.4.4) are shown for merging clusters (black rectangular) and for clusters with RH (red rectangular). These values of ξ_{\min} both constrain $\tau_m \sim \tau_{RH} \sim 2.5 - 3$ Gyr (this is also show in the Figure).

virial radius of the main cluster (that for our clusters is $\sim 2 - 3$ Mpc). However, since we are considering a “rate”, number of infalling halos per unit time, what is important is that the halos crossing the virial radius of the main cluster cross, at a given time, the radius of 500 kpc reaching the central regions. According to cosmological simulations, halos with a mass ratio $\xi \gtrsim 0.1$ reach their pericentric distance, that is $\sim 0.2 - 0.3 R_v$, within a time-scale of ~ 0.9 Gyr from the virial crossing (e.g., Tormen et al. 2004).

The other assumption is that of binary mergers, *i.e.*, we assume that the disturbance we measure in the X-rays is mainly caused by a binary merger event between the two main progenitors. Consequently, we derive the expected average merger fraction from the fitting formulae by FMB10 assuming that in a merger timescale there is a main binary merger event with $\xi \gtrsim \xi_{\min}$ that influence the observed dynamical status. However, in a merger timescale, especially for long timescale, clusters might experience multiple merger episodes characterized by lower mass ratio ($\xi < \xi_{\min}$). If the number of mergers with a mass ratio slightly smaller than ξ_{\min} is significant, our assumption would be no longer valid, since also the interplay of these mergers would contribute to the morphological disturbance.

4.2. Mergers and observed X-ray morphology

Given these premises, we proceed with the comparison between the observed merger fraction and the results by FMB10. From Fig. 1 it is clear that we can find combinations (τ_m , ξ_{\min}) for which the expected merger fraction can match that observed in our sample. Fig.2 (black region) shows the allowed regions of

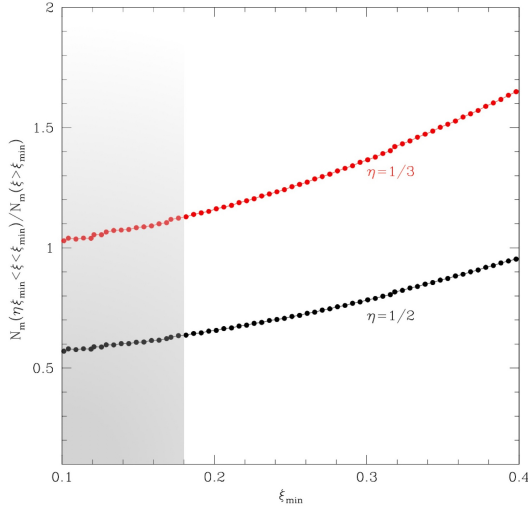


Fig. 3. Ratio between the number of mergers with $\eta \xi_{\min} < \xi < \xi_{\min}$ and that with $\xi \geq \xi_{\min}$, for $\eta = 1/2$ (bottom black dots) and $\eta = 1/3$ (upper red dots). The shadowed region indicate the range of $\xi_{\min} = 0.1 - 0.18$ constrained by the merger timescale derived from numerical simulations (Tormen et al. 2004).

(τ_m, ξ_{\min}) that is derived by matching theory and observations. As expected, there is a clear degeneracy between τ_m and ξ_{\min} .

We first identify forbidden regions in the τ_m - ξ_{\min} diagram. A lower limit on τ_m can be obtained by assuming that the merger-driven perturbations within a region of diameter 1 Mpc cannot last for a timescale shorter than the sound crossing time of that region, that for a galaxy cluster with $T \sim 10^8$ K is $\tau_{\text{sound}} \approx 1$ Gyr. We note that values of τ_m constrained by the observations are always larger than τ_{sound} (at least for $\xi_{\min} \geq 0.05$). An upper bound to τ_m can be derived by considering the fact that extremely large duration of mergers would make dynamically disturbed all the clusters that are observed at a given cosmic epoch. Specifically, for each cluster of the sample with mass M_0 at redshift z_0 we derive the values of $\tau_{m,\text{max}}$, as a function of the progenitor mass ratio ξ_{\min} , corresponding to the redshift z for which Eq. 2 gives $N_m = 1$. This means that a merger event with $\xi \geq \xi_{\min}$ is still producing a disturbance in all clusters of our sample at the epoch of observation. The derived distribution of $\tau_{m,\text{max}}$, for each value of ξ_{\min} , and its mean value are reported in Fig.2 (blue region and line, respectively). We note that values of τ_m constrained by the observations are always smaller than $\tau_{m,\text{max}}$.

Due to the degeneracy between τ_m and ξ_{\min} in principle large merger timescales can be admitted to explain the observed merger fraction. However, as already anticipated, under this condition our hypothesis of binary mergers can be no longer valid since multiple merger events with mass ratio slightly smaller than ξ_{\min} can contribute to the disturbance. To check this hydrodynamical simulations are necessary to unambiguously relate the merger mass ratio to the cluster morphological parameters, but this is beyond the scope of the paper and deserves future *ad hoc* simulations. Here we limit at the following test. In Fig.3 we use the values (τ_m, ξ_{\min}) constrained in Fig.2 and show the ratio between the number of mergers with mass ratio in the range $\eta \xi_{\min} - \xi_{\min}$ and that of mergers with $\xi \geq \xi_{\min}$; $\eta = 1/2$ and $1/3$ are considered. We conclude that the binary approach adopted in our paper is appropriate for merger timescale as large as 3 – 4 Gyr (those corresponding to $\xi_{\min} \sim 0.2 - 0.3$).

A possibility to break the degeneracy between τ_m and ξ_{\min} is to adopt values of τ_m inferred from numerical simulations. A reference timescale is the time necessary to a subcluster to

complete an orbit around the center of mass of the main cluster. Following Tormen et al. (2004) this time can be estimated as $2 \times (\tau_a - \tau_p)$, where $\tau_a = \tau_a(\xi) = 1.6(\xi + 0.02)^{-0.17}$ Gyr and $\tau_p = 0.9$ Gyr are the apocentric and pericentric timescale, respectively. This timescale is reported in Fig. 2 (green line) as a function of ξ_{\min} . It intercepts the region constrained by the observations for $\tau_m \approx 2.5$ Gyr implying $\xi_{\min} \approx 0.14$. In Tormen et al. (2004), τ_a and τ_p are derived from analytic fits to the results of numerical simulations, we note however that the dispersion around the median value is ~ 0.5 Gyr. As a consequence the merger timescale is constrained as $\tau_m \sim 2 - 3$ Gyr, implying $\xi_{\min} \sim 0.1 - 0.18$. Coming back to Fig.3 we note that for $\xi_{\min} \approx 0.1 - 0.18$ (shadowed region) the number of mergers with mass ratio $1/3 \xi_{\min} < \xi < \xi_{\min}$ is about the same of that of mergers with $\xi \geq \xi_{\min}$ and that the number of mergers with $1/2 \xi_{\min} < \xi < \xi_{\min}$ is about half of that of mergers with $\xi \geq \xi_{\min}$. These mergers being characterized by relatively small mass ratio ($\xi \sim 0.03 - 0.09$) and being not numerous should have a negligible influence on the cluster morphological parameters, thus our assumption of binary mergers is reasonably correct.

4.3. Mergers and Radio Halos

RH are always observed in dynamically disturbed systems. However they are found only in a fraction of the clusters that are classified as merging systems. In this Section we follow the approach already adopted in Sect. 4.2 and attempt to constrain the properties that cluster mergers should have in order to explain the observed fraction of clusters with RH. In Fig. 2 we report the region (τ_m, ξ_{\min}) constrained by requiring that the predicted merger fraction matches the observed fraction of clusters with RH (red shadowed region). At this point we can adopt two main scenarios:

- i) we can assume that the lifetime of RH is equivalent to the lifetime of the merger-induced disturbances identified by X-ray parameters. Under this hypothesis and since RH are found in disturbed systems, we can assume that RH are generated in those systems that have larger mass ratios among merging clusters in our sample. In this case we derive $\xi_{\min} \sim 0.18 - 0.25$ for $\tau_m = 2 - 3$ Gyr as constrained in Sect.4.3.
- ii) we can assume that RH are statistically generated in “all” mergers identified in our sample, but they are short-living compared to the timescale of the merger-induced disturbance. Under this assumption the lifetime of RH is simply $\tau_{RH} \sim \tau_m \times (f_{RH}/f_m) \sim (0.7 - 0.8)\tau_m$, i.e., $\tau_{RH} \sim 1.4 - 2.4$ Gyr for $\tau_m = 2 - 3$ Gyr.

4.4. Constraints on ξ_{\min} from observations

The mass ratio ξ_{\min} is a simple outcome of our procedure that is appropriate for binary mergers. However this value can be constrained independently by observations of clusters in our sample. Observations of single clusters may be used to derive independent constraints on ξ . We collected information in the literature about the mass ratio of the merging clusters of our sample. These mass ratio are derived from optical/near-IR observations of galaxy clusters through the weak lensing analysis or through the study of the galaxy velocity distributions in the clusters (see Tab. A.1). We found information for 7 clusters with RH and for Z5247 that hosts a “candidate” RH (see Tab. A.1). For 5 merging clusters without RH, we have looked at the reconstructed convergence maps from weak gravitational lensing (see Tab. A.1). For these clusters we have estimated the mass ratio of the dif-

ferent merging components adopting circular filters on the reconstructed convergence maps with a typical scale that allows to isolate the different correlated peaks. Due to the restricted number density of sources beyond the clusters from which the weak lensing signal is measured and so to the limited resolution of the recovered convergence maps – around the arcmin scale – we stress that in these cases the quoted values represent an upper limit for the mass ratio.

The minimum values of ξ we found for merging clusters in our sample is $\sim 0.14 - 0.16$. If we use these values, $\xi_{\min} \sim 0.14 - 0.16$ (black rectangular region in Fig. 2), we can derive $\tau_m \approx 2.5 - 3$ Gyr, consistent with the reference values of merging timescales derived from results of cosmological simulations (see Fig. 2).

We found some evidence (the information is available only for half of the merging clusters in the sample) that merging clusters with RH are in general characterized by mergers with larger mass ratio than merging clusters without RH: ξ ranges from $\xi \sim 0.2 - 0.25$ up to $\xi \sim 1$. If we assume $\xi_{\min} \sim 0.2 - 0.25$ for merging clusters with RH (red rectangular region in Fig. 2), we constrain $\tau_{RH} \sim \tau_m \sim 2.5 - 3$ Gyr, thus in this case the RH lifetime would be comparable with the merger timescale, potentially supporting the scenario i) in Sect.4.3.

5. Summary and Discussion

Observations establish a clear connection between RH and mergers (e.g., Cassano et al. 2010), suggesting that RH can be used as probes of cluster merging rate with cosmic time. Based on this possibility, in this paper we carry out an exploratory study. By combining the observed fraction of merging clusters and the observed fraction of RH in clusters with the merging rate predicted by fitting formulae based on cosmological simulations we attempt to infer constraints on merger properties of clusters that appear disturbed in X-rays and of clusters that host RH.

We use the Planck SZ cluster catalogue (PSZ; Planck Collaboration XXIX 2014a) and select a sample of 54 clusters with mass $M_{500} \geq 6 \times 10^{14} M_{\odot}$ and redshift $0.2 \leq z \leq 0.33$. 39 of these clusters have both X-ray and radio information and represent a sub-sample that can be used to measure the fraction of RH and that of merging clusters. Mergers in the sample are identified by means of X-ray morphological parameters. We find that all RH are in merging clusters whereas not all merging clusters host a RH, specifically $\sim 44 - 51\%$ of the clusters in the sample have a RH, while (using Chandra and XMM-Newton X-ray data) the total fraction of merging clusters is $\sim 62 - 67\%$.

We convert the theoretical merging rate per halo (FMB10), that mainly depends on the mass ratio of the two progenitors, $\xi = M_i/M_1 < 1$, into merger fraction by adopting a merger time scale τ_m as a free parameter. The predicted fraction of merging clusters has a strong dependence on ξ_{\min} , i.e., the minimum mass ratio of the mergers (larger is ξ_{\min} smaller is the number of mergers; Fig. 1) and on τ_m (larger is τ_m larger is the expected fraction of merging clusters; Fig. 1). The comparison between the observed and predicted merger fraction allows to constrain a allowed region in the diagram (ξ_{\min} , τ_m) where there is degeneracy between these two parameters (Fig. 2).

We attempt to break the degeneracy between ξ_{\min} and τ_m :

a) by assuming the merger timescale that is derived by cosmological simulations (e.g., Tormen et al. 2004), $\tau_m \sim 2 - 3$ Gyr, we find that a value $\xi_{\min} \sim 0.1 - 0.18$ explains the observed merger fraction;

b) by assuming values of ξ_{\min} derived through the analysis of optical/near-IR observations of merging clusters in the sample:

$\xi_{\min} \sim 0.14 - 0.16$ we find that a merger timescale $\tau_m \approx 2.5 - 3$ Gyr explains the observed merger fraction.

Interestingly, values of the parameters that are obtained independently in a) and b) are consistent.

We find that all clusters with RH in our sample are merging systems but that not all merging clusters host a RH. There are two main possibility to interpret this difference:

- *Scenario 1*) RH have lifetime similar to the lifetime of merger-driven disturbances in the X-rays, but they are generated in the merging events with larger mass ratio. Values of mass ratio derived from optical/near-IR observations of galaxy clusters in the sample (through weak lensing analysis or through the study of the velocity distribution of galaxies in the clusters) may support this possibility. Indeed we find that ξ ranges between $\sim 0.2 - 0.25$ and ~ 1 for RH clusters, whereas values of $\xi \sim 0.14 - 0.16$ up to $\xi \sim 0.25 - 0.3$ are found for merging clusters without RH. If we assume $\xi_{\min} \sim 0.2 - 0.25$, we find that $\tau_{RH} \sim \tau_m \approx 2 - 2.5$ Gyr should be adopted to explain the observed RH fraction.

- *Scenario 2*) the lifetime of RH (τ_{RH}) is shorter than the timescale of merger-induced disturbance in the X-rays, with $\tau_{RH} \sim \tau_m \times (f_{RH}/f_m) \sim (0.7 - 0.8)\tau_m$. In this case assuming no difference between the mass ratio of clusters with and without RH, we find $\tau_{RH} \sim 1.4 - 2.4$ Gyr.

In general, we note that both different timescales ($\tau_{RH} \lesssim \tau_m$; i.e., *Scenario 2*) and mass ratios (i.e., *Scenario 1*) are likely to govern the statistic of giant RH.

This study deals with several limitations and is based on simplified assumptions:

i) the observed fraction of merging clusters is derived by measuring the fraction of clusters with significant X-ray disturbance, this means that we are sensitive only to merger episodes with relevant mass accretion;

ii) while observationally, the fraction of merging clusters is derived by measuring the morphological disturbances of clusters in the sample on a circular region of ~ 1 Mpc (diameter), the theoretical merging rate (FMB10) and hence the merger fraction is derived by considering all the infalling halos within the virial radius ($\sim 2 - 3$ Mpc) of the main clusters. However, it should be mentioned that numerical simulations allow to argue that for $\xi \gtrsim 0.1$ the two rates should be comparable (see Sect.4 and Tormen et al 2004 for more details);

iii) we assume that the X-ray disturbance that we measure in the X-rays is mainly caused by a binary merger event, specifically by the one with larger mass ratio. Thus in deriving the expected merger fraction from theoretical fitting formulae we attempt to select the values of ξ_{\min} that matches the merger fraction assuming that mergers with smaller mass ratio do not play a role. However, in principle, in the timescale of the merger-induced disturbance, τ_m , clusters might experience multiple merger episodes with slightly lower mass ratio that can contribute to the morphological disturbance. We show that for typical merger timescale (constrained by simulations and by the observed value of ξ_{\min}) the contribution of these slightly minor mergers is expected to be not relevant. Clearly, *ad hoc* simulations and follow up studies are necessary to establish a more solid connection between mergers and X-ray disturbances.

It is currently thought that giant RH are generated as a consequence of the acceleration of relativistic electrons by the MHD turbulence stirred up in the ICM by cluster-cluster mergers (e.g., Brunetti & Jones 2014). In this framework the *scenario 1*) discussed above implies that the timescale of the X-ray merger-induced disturbances and that of the turbulent stirring of the ICM by cluster mergers in the central 1 Mpc (diameter) region are similar. These timescales are shorter than the dynamical

time-scale of the merger which is defined as the time interval between the moment when the center of the less massive cluster first crosses the virial radius of the main one and the moment when the final system reaches a relaxed state. As a consequence, in this scenario RH are not switched on at the beginning of the merger but after a time period that is necessary to the infalling subcluster to generate ICM turbulence in the central Mpc region (~ 0.9 Gyr; see Sect.4.1). Since gravity drives mergers between galaxy clusters, it is expected that the turbulent energy budget should scale with the cluster thermal energy. As a consequence, very massive and merging systems should be the natural host of Mpc-scale RH (e.g., Cassano & Brunetti 2005; Vazza et al. 2006, 2011; Paul et al. 2011). In line with these expectations we find $f_{RH} \approx 44 - 51\%$ for clusters with $M_{500} \gtrsim 6 \times 10^{14} M_{\odot}$ at $0.2 \lesssim z \lesssim 0.33$ (see also Sommer & Basu 2014; Cuciti et al. 2015). Also the mass-ratio may play a role because major mergers are more powerful events and have the potential to generate more turbulence in larger volumes. For instance, using a semi-analytic approach, Cassano & Brunetti (2005) showed that, for a given cluster mass, the ratio between the turbulent energy and the cluster thermal energy increases with increasing ξ , becoming smaller than 5% for $\xi < 0.2$ (see also Fig.3 in Cassano & Brunetti 2005). This can explain the absence of RH in clusters undergoing merger events with mass ratio $\xi < 0.2$.

On the other hand, *scenario 2*) would imply that mergers drive turbulent re-acceleration of relativistic particles in the ICM on a timescale that is $\sim 0.7 - 0.8$ shorter than the timescale duration of the morphological disturbances in the X-rays. Lagrangian (SPH) simulations of two colliding idealized clusters have been used to study the time-evolution of the RH emission during mergers (Donnert et al. 2013). These simulations predict shortly living RH that are generated after the first core passage and fading within $\lesssim 1$ Gyr timescale. In fact, this timescale is shorter than that constrained assuming the *scenario 2*), however this can be due to the idealized setup of the model and it is very likely that the lifetime of RH is significantly larger in a cosmological context. High resolution cosmological simulations also show an increase of the turbulence (both compressible and incompressible) and of the acceleration rate during major mergers (Miniati 2015). These simulations add also important information as they allow to evaluate the ratio τ_{RH}/τ_m under different assumptions about the ICM microphysics. This is an important point as it implies that statistical studies of the connection between RH and merging rates combined with numerical simulations have also the potential to put fundamental constraints on the ICM microphysics and acceleration mechanisms (Miniati 2015, Brunetti 2016).

To conclude, while it is clear that massive and merging clusters are the natural hosts of giant RH, the presence of merging clusters without RH pose fundamental questions: is there a role of the merger mass ratio in the formation of giant RH? which is the lifetime of RH with respect to the merger timescale? is the RH lifetime tied by the microphysics of the ICM?

Our exploratory study has shown that meaningful values of the merger parameters can be derived combining the observed fraction of RH and the theoretical merging rate in the LCDM model. More specifically our results seem to suggest that the mass-ratio may play a role in the generation of RH, however this result is not conclusive and we cannot conclude whether *scenario 1*) is favored with respect to *scenario 2*), or whether mass ratios and different timescales both play a role. An important step forward to address the lifetime of RH and the connection with mergers can be achieved by increasing the statistic of merging clusters without RH. Our study is limited by current data

that allow to infer these constraints only in very massive clusters at relatively low redshifts. In fact in our study we use the currently most complete mass-selected sample of galaxy clusters with radio and X-ray information that, however, is limited to very massive ($M_{500} \gtrsim 6 \times 10^{14} M_{\odot}$) and relatively nearby systems ($z \approx 0.2 - 0.33$). Based on energy arguments the occurrence of “radio quiet” merging clusters should increase at smaller masses (or at higher redshifts or small mass-ratio mergers; e.g., Cassano et al. 2006). Thus extending the samples of clusters at smaller masses (or at higher redshift) is necessary to obtain stronger constraints on the physical conditions necessary to generate RH. This will be possible with the upcoming new generation of radio facilities, such as LOFAR, ASKAP, MeerKAT up to SKA1 (e.g., Cassano et al. 2015). Future surveys also offer the possibility to explore the frequency dependence of the occurrence of RH in galaxy clusters. Current models predict the presence of RH with ultra-steep radio spectra (USSRH) especially in low massive (or high- z) galaxy clusters (e.g., Cassano et al. 2006; Brunetti et al. 2008). As a consequence, it is possible that some of the merging clusters without RH host actually USSRH and observations with LOFAR (and SKA1-LOW in the future) will be crucial to check this possibility.

Acknowledgements. We thank the referee for the valuable report. S.E. acknowledges support from ASI-INAF n.1/009/10/0 and NuSTAR-ASI/INAF n. 1/037/12/0. GB and RC acknowledge partial support from PRIN-INAF 2014. GB acknowledges support from the Alexander von Humboldt Foundation. We thank K. Dolag for useful discussion and V. Cuciti for providing the morphological parameters of 5 clusters (marked with *** in Tab.A1).

References

- Bacchi, M., Feretti, L., Giovannini, G., & Govoni, F. 2003, *A&A*, 400, 465
- Bardeau, S., Soucail, G., Kneib, J.-P., et al. 2007, *A&A*, 470, 449
- Barrena, R., Boschini, W., Girardi, M., & Spolaor, M. 2007, *A&A*, 467, 37
- Barrena, R., Girardi, M., Boschini, W., De Grandi, S., & Rossetti, M. 2014, *MNRAS*, 442, 2216
- Basu, K. 2012 *MNRAS*, 421L, 112
- Böhringer, H., Pratt, G. W., Arnaud, M., et al., 2010, *A&A*, 514, 32
- Bonafede, A., Intema, H., Brüggen, M., et al. 2015, *MNRAS*, 454, 3391
- Boschini, W., Girardi, M., Spolaor, M., & Barrena, R. 2006, *A&A*, 449, 461
- Boylan-Kolchin, M., Springel, V., White, S. D. M., Jenkins, A., & Lemson, G. 2009, *MNRAS*, 398, 1150
- Brüggen, M., Bykov, A., Ryu, D., Röttgering, H. 2012, *Space Sci. Rev.*, 166, 187
- Brüggen, M., & Vazza, F. 2015, *Magnetic Fields in Diffuse Media*, 407, 599
- Brunetti, G. 2016, *Plasma Physics and Controlled Fusion*, 58, 014011
- Brunetti G., Venturi, T., Dallacasa, D., Cassano, R., Dolag K., Giacintucci, S., Setti, G., 2007, *ApJ Letter*, 670, L5
- Brunetti, G., & Lazarian, A. 2007, *MNRAS*, 378, 245
- Brunetti, G., Giacintucci, S., Cassano, R. et al. 2008, *Nature*, 455, 944
- Brunetti G., Cassano, R. Dolag, K., Setti, G. 2009, *A&A*, 507, 661
- Brunetti, G., & Jones, T. W. 2014, *International Journal of Modern Physics D*, 23, 1430007
- Buote, D. A. & Tsai, J. C. 1995, *ApJ*, 452, 522
- Cassano, R., & Brunetti, G. 2005, *MNRAS*, 357, 1313
- Cassano, R., Brunetti, G., & Setti, G. 2006, *MNRAS*, 369, 1577
- Cassano, R., Ettori, S., Giacintucci, S., et al. 2010, *ApJ*, 721, L82
- Cassano, R., Ettori, S., Brunetti, G., Giacintucci, S., Pratt, G. W. et al. 2013, *ApJ*, 777, 141
- Cassano, R., Bernardi, G., Brunetti, G., et al. 2015, *Advancing Astrophysics with the Square Kilometre Array (AASKA14)*, 73
- Conselice, C. J. 2014, *ARA&A*, 52, 291
- Conselice, C. J., Bershad, M. A., Dickinson, M., & Papovich, C. 2003, *AJ*, 126, 1183
- Cuciti, V., Cassano, R., Brunetti, G., et al. 2015, *A&A*, 580, A97
- Dahle, H., Kaiser, N., Irgens, R. J., Lilje, P. B., & Maddox, S. J. 2002, *ApJS*, 139, 313
- De Boni, C., Serra, A. L., Diaferio, A., Giocoli, C., & Baldi, M. 2016, *ApJ* 818, 188
- De Propriis, R., Liske, J., Driver, S. P., Allen, P. D., & Cross, N. J. G. 2005, *AJ*, 130, 1516
- Diaferio, A. 2015, *arXiv:1502.01195*
- Donnert, J., Dolag, K., Brunetti, G., & Cassano, R. 2013, *MNRAS*, 429, 3564

- Duffy, A. R., Schaye, J., Kay, S. T., & Dalla Vecchia, C. 2008, MNRAS, 390, L64
- Ettori, S., Gastaldello, F., Leccardi, A., et al. 2010, A&A, 524, A68
- Fakhouri, O., & Ma, C.-P. 2008, MNRAS, 386, 577
- Fakhouri, O., Ma, C.-P., & Boylan-Kolchin, M. 2010, MNRAS, 406, 2267
- Feretti, L., Fusco-Femiano, R., Giovannini, G., & Govoni, F. 2001, A&A, 373, 106
- Feretti, L., Giovannini, G., Govoni, F., Murgia, M. 2012, A&ARv, 20, 54
- Giacintucci, S., Venturi, T., Cassano, R., Dallacasa, D., & Brunetti, G. 2009, ApJ, 704, L54
- Giacintucci, S., Dallacasa, D., Venturi, T., et al. 2011, A&A, 534, A57
- Giacintucci, S., Kale, R., Wik, D. R., Venturi, T., & Markevitch, M. 2013, ApJ, 766, 18
- Giovannini, G., Feretti, L., Govoni, F., Murgia, M., & Pizzo, R. 2006, Astronomische Nachrichten, 327, 563
- Giocoli, C., Moreno, J., Sheth, R. K., & Tormen, G. 2007, MNRAS, 376, 977
- Giocoli, C., Tormen, G., & Sheth, R. K. 2012, MNRAS, 422, 185
- Govoni, F., Enßlin, T. A., Feretti, L., Giovannini, G., 2001, A&A 369, 441
- Govoni, F., Murgia, M., Giovannini, G., Vacca, V., & Bonafede, A. 2011, A&A, 529, A69
- Guo, Q., & White, S. D. M. 2008, MNRAS, 384, 2
- Hopkins, P. F., Cox, T. J., Hernquist, L., et al. 2013, MNRAS, 430, 1901
- Jian, H.-Y., Lin, L., & Chiueh, T. 2012, ApJ, 754, 26
- Kale, R., & Parekh, V. 2016, MNRAS,
- Kale, R., Venturi, T., Giacintucci, S., et al. 2013, A&A, 557, A99
- Kale, R., Venturi, T., Giacintucci, S., et al. 2015, A&A, 579, A92
- Kravtsov, A. V., & Borgani, S. 2012, ARA&A, 50, 353
- Kulsrud, R. M., Cen, R., Ostriker, J. P., & Ryu, D. 1997, ApJ, 480, 481
- Landry, D., Bonamente, M., Giles, P., et al. 2013, MNRAS, 433, 2790
- Lemze, D., Postman, M., Genel, S., et al. 2013, ApJ, 776, 91
- Lotz, J. M., Primack, J., & Madau, P. 2004, AJ, 128, 163
- Lotz, J. M., Jonsson, P., Cox, T. J., et al. 2011, ApJ, 742, 103
- Mahdavi, A., Hoekstra, H., Babul, A., Balam, D. D., & Capak, P. L. 2007, ApJ, 668, 806
- Mantz, A. B., Allen, S. W., Morris, R. G., et al. 2015, MNRAS, 449, 199
- Miniati, F. 2015, ApJ, 800, 60
- Mohr, J. J., Fabricant, D. G., Geller, M. J. 1993, ApJ, 413, 492
- McBride, J., Fakhouri, O., & Ma, C.-P. 2009, MNRAS, 398, 1858
- Moreno, J., Giocoli, C., & Sheth, R. K. 2008, MNRAS, 391, 1729
- Murgia, M., Govoni, F., Markevitch, M., et al. 2009, A&A, 499, 679
- Navarro, J. F., Frenk, C. S., & White, S. D. M. 1997, ApJ, 490, 493
- Norman, M. L., & Bryan, G. L. 1999, The Radio Galaxy Messier 87, 530, 106
- Okabe, N., & Umetsu, K. 2008, PASJ, 60, 345
- Okabe, N., Takada, M., Umetsu, K., Futamase, T., & Smith, G. P. 2010, PASJ, 62, 811
- Parekh, V., van der Heyden, K., Ferrari, C., Angus, G., & Holwerda, B. 2015, A&A, 575, A127
- Patton, D. R., Carlberg, R. G., Marzke, R. O., et al. 2000, ApJ, 536, 153
- Paul, S., Iapichino, L., Miniati, F., Bagchi, J., & Mannheim, K. 2011, ApJ, 726, 17
- Planck Collaboration, Ade, P. A. R., Aghanim, N., et al. 2014a, A&A, 571, A29
- Planck Collaboration, Ade, P. A. R., Aghanim, N., et al. 2014b, A&A, 571, A20
- Poole, G. B., Fardal, M. A., Babul, A., et al. 2006, MNRAS, 373, 881
- Reid, A. D., Hunstead, R. W., Lemonon, L., & Pierre, M. M. 1999, MNRAS, 302, 571
- Ricker, P. M., & Sarazin, C. L. 2001, ApJ, 561, 621
- Rossetti, M., Eckert, D., Cavalleri, B. M., et al. 2011, A&A, 532, A123
- Santos, J. S., Rosati, P., Tozzi, P., Böhringer, H., Ettori, S., Bignamini, A. 2008, A&A, 483, 35
- Sommer, M. W., Basu, K. 2014, MNRAS, 437, 2163
- Soucail, G. 2012, A&A, 540, A61
- Springel, V., White, S. D. M., Jenkins, A., et al. 2005, Nature, 435, 629
- Subramanian, K., Shukurov, A., & Haugen, N. E. L. 2006, MNRAS, 366, 1437
- Tormen, G., Moscardini, L., & Yoshida, N. 2004, MNRAS, 350, 1397
- Vazza, F., Tormen, G., Cassano, R., Brunetti, G., & Dolag, K. 2006, MNRAS, 369, L14
- Vazza, F., Brunetti, G., Gheller, C., Brunino, R., & Brügggen, M. 2011, A&A, 529, A17
- Venturi, T., Giacintucci, S., Brunetti, G., et al. 2007, A&A, 463, 937
- Venturi, T., Giacintucci, S., Dallacasa, D., Cassano, R., Brunetti, G. et al. 2008, A&A, 484, 327
- Venturi, T., Giacintucci, G., Dallacasa, D., et al. 2011, MNRAS, 414, L65
- van den Bosch, F. C. 2002, MNRAS, 331, 98
- Wen, Z. L., & Han, J. L. 2015, MNRAS, 448, 2
- Yuan, Z. S., Han, J. L., & Wen, Z. L. 2015, ApJ, 813, 77
- Wittman, D., Dawson, W., & Benson, B. 2014, MNRAS, 437, 3578
- Ziparo, F., Braglia, F. G., Pierini, D., et al. 2012, MNRAS, 420, 2480

Appendix A: Additional Tables

In Tab.A.1 we report the main properties of the 54 clusters belonging to our sample, specifically: Col.(1) cluster's name; Col.(2) cluster's redshift; Col.(3) M_{500} from Planck Collaboration 2014; Col.(4) virial mass, M_{vir} (see Sect. 2); Col.(5) information about the presence of diffuse radio emission; Col.(6) cluster dynamical status; Col.(7) mass ratio, when available. The first two panels contain the 39 clusters with both radio and X-ray information (clusters with RH are in the second panel); the third panel contains clusters with X-ray information; the three clusters in the forth panel are those without radio and X-ray information. In Tab.A.2 we report the morphological parameters derived for the 41 clusters with Chandra X-ray data (see Sect. 2): P_3/P_0 , w and c , with their inferior and superior values ($[P_3/P_0 - 1\sigma$, $P_3/P_0 + 1\sigma]$, and so on for the others).

Table A.1. Cluster's properties

cluster name	z	M_{500} [$10^{14} M_{\odot}$]	M_{vir} [$10^{14} M_{\odot}$]	radio info	X-ray info	mass ratio ^z
clusters with radio and X-ray data						
A2697	0.23	6.00	11.00	UL ^a	relaxed ¹	–
A3088	0.25	6.71	12.25	UL ^a	relaxed ²	–
A2667	0.23	6.81	12.46	UL ^a	relaxed ³	–
RXJ0142.0+21	0.28	6.07	10.95	UL ^b	relaxed ²	–
A1423	0.21	6.09	11.08	UL ^a	relaxed ³	–
A1576	0.30	5.98	10.8	UL ^b	relaxed ^{2,*,**}	1:4-1:3 (Dahle et al. 2002)
A2261	0.22	7.39	13.56	UL ^b	relaxed ³	–
A2537	0.30	6.17	11.15	UL ^a	relaxed ³	–
S0780	0.24	7.71	14.22	MH ^c	relaxed ³	–
A1835	0.25	8.46	15.53	MH ^d	relaxed ⁴	–
A2390	0.23	9.48	17.59	MH ^e	relaxed ³	–
RXCJ1504.1-02	0.22	6.98	12.80	MH ^f	relaxed ³	–
A3444	0.25	7.62	13.98	MH ^c	relaxed ⁴	–
A68	0.26	6.19	11.25	UL ^c	merger ⁴	1:6-1:5 (Okabe et al. 2010)
A2631	0.28	6.97	12.75	UL ^a	merger ³	1:7-1:6 (Okabe et al. 2010)
A781	0.30	6.36	11.50	UL ^{a,ax}	merger ³	1:3 (Wittman et al. 2014)
A1763	0.23	8.29	15.25	no RH ^a	merger ⁴	1:5-1:4 (Bardeau et al. 2007)
PSZ1 G205.07-62.94	0.31	7.37	13.40	no RH ^g	merger ¹	–
A2744	0.31	9.56	17.48	RH ^h	merger ³	1:3 (Boschin et al. 2006)
A209	0.21	8.17	15.02	RH ⁱ	merger ³	–
A2163	0.20	16.44	31.52	RH ^j	merger ³	1:3 (Soucail 2012)
RXCJ2003.5-2323	0.32	7.48	13.57	RH ⁱ	merger ³	–
A520	0.20	7.06	13.06	RH ^h	merger ³	1:1 (Mahdavi et al. 07)
A773	0.22	7.08	13.05	RH ^h	merger ³	1:4-1:10 (Barrera et al. 2007)
A1758a	0.28	7.99	14.68	RH ^m	merger ³	1:2 (Okabe et al. 2008)
A1351	0.32	7.14	12.95	RH ⁿ	merger ⁴	1:5 (Barrera et al. 2014)
A2219	0.23	11.01	20.40	RH ^e	merger ³	–
A521	0.25	6.91	12.37	RH ^o	merger ³	–
A697	0.28	11.48	21.37	RH ^a	merger ³	–
PSZ1 G171.96-40.64	0.27	11.13	20.88	RH ^p	merger ¹	–
A1300	0.31	8.83	16.15	RH ^q	merger ³	1:1 (Ziparo et al. 2011)
RXC J1314.4-2515	0.24	6.15	11.20	RH ⁱ	merger ¹	–
RXC J1514.9-1523	0.22	8.34	15.35	RH ^f	merger ⁴	–
A1682	0.23	6.20	11.33	RH ^a	merger ³	–
A1443	0.27	7.74	14.15	RH ^s	merger ^{***}	–
Z5247	0.23	6.04	11.00	RH ^{?c}	merger ⁴	1:4 (Dahle et al. 2002)
A2552	0.30	7.53	13.65	RH ^{?c}	relaxed ^{?4,*}	–
RXC J0510.7-0801	0.22	7.36	13.50	RH ^{?c}	merger ^v	–
A402	0.32	7.20	13.06	MH ^{?r}	relaxed ^{d***}	–
clusters with (only) X-ray data						
A2895	0.23	6.15	11.22	–	merger ^v	–
A2813	0.29	9.16	15.15	–	merger ^v	–
PSZ1G139.61+24	0.27	7.09	12.93	–	relaxed ^{d***}	–
A2355	0.23	6.92	12.75	–	merger ^{***}	–
A1733	0.26	7.05	12.85	–	merger ^{***}	–
MACS J2135-010	0.33	7.57	13.8	–	merger ^v	–
RXC J2051.1+0216	0.32	6.13	11.07	–	merger ¹	–
A2472	0.31	6.15	11.12	–	merger ¹	–
A56	0.30	6.20	11.25	–	merger ¹	–
A384	0.24	6.38	11.65	–	relaxed ¹	–
RXCJ1322.8+31	0.31	6.63	12.0	–	relaxed ¹	–
PSZ1 G019.12+3123	0.28	7.08	12.95	–	merger ¹	–
clusters without radio and X-ray data						
ZwCl 1028.8+1419*	0.31	6.11	11.05	–	–	–
A3041*	0.23	6.12	11.24	–	–	–
A220*	0.33	6.74	12.20	–	–	–

Notes – radio info.: ^a Venturi et al. 2008; ^b Kale et al. 2013; ^c Kale et al. 2015; ^d Murgia et al. 2009; ^e Bacchi et al. 2003; ^f Giacintucci et al. 2011; ^g Ferrari et al. (private communication); ^h Govoni et al. 2001; ⁱ Venturi et al. 2007; ^j Feretti et al. 2001; ^m Giovannini et al. 2006; ⁿ Giacintucci et al. 2009; ^o Brunetti et al. 2008; ^p Giacintucci et al. 2013; ^q Reid et al. 1999; ^r Macario et al. (private communication); ^s Bonafede et al. 2015. X-ray info.: ¹ from XMM-Newton visual inspection; ² Cassano et al. 2013; ³ Cassano et al. 2010; ⁴ Cuciti et al. 2015; ^v this paper. ^{ax} Venturi et al. (2011) report on a possible RH in A781, however those observations were not conclusive (see also Govoni et al. 2011). * Landry et al. (2013) classify these clusters as “unrelaxed” systems; ** Dahle et al. (2002) report on some merger activity in this cluster. ^z the mass ratio here is defined as $1/\xi$. *** V. Cuciti, private communication.

Table A.2. Cluster's morphological parameters

cluster name	P_3/P_0 [min, max] [10^{-7}]	w [min, max] [10^{-2}]	c [min, max]
A3088	0.833 [0.279, 1.663]	0.285 [0.220, 0.370]	0.339 [0.332, 0.345]
A2667	1.395 [0.799, 2.152]	0.927 [0.800, 1.030]	0.407 [0.402, 0.410]
RXJ0142.0+21	6.625 [3.655, 10.350]	0.738 [0.650, 0.910]	0.186 [0.180, 0.191]
A1423	1.413 [0.656, 3.880]	0.562 [0.460, 0.760]	0.331 [0.323, 0.342]
A1576	5.950 [3.661, 11.071]	1.271 [0.940, 1.590]	0.235 [0.226, 0.241]
A2261	1.026 [0.513, 1.673]	0.495 [0.430, 0.570]	0.334 [0.330, 0.337]
A2537	0.351 [0.165, 1.208]	0.561 [0.460, 0.660]	0.278 [0.273, 0.282]
S0780	0.480 [0.243, 0.801]	0.827 [0.760, 0.880]	0.473 [0.470, 0.476]
A1835	0.459 [0.317, 0.576]	0.996 [0.952, 1.032]	0.487 [0.485, 0.488]
A2390	0.694 [0.520, 0.933]	1.171 [1.120, 1.200]	0.305 [0.303, 0.306]
RXCJ1504.1-02	0.148 [0.086, 0.221]	0.459 [0.430, 0.490]	0.624 [0.622, 0.626]
A3444	0.434 [0.256, 0.650]	0.745 [0.683, 0.806]	0.465 [0.461, 0.467]
A68	3.199 [1.368, 7.026]	1.004 [0.740, 1.240]	0.149 [0.141, 0.157]
A2631	1.550 [0.647, 5.941]	1.570 [1.270, 1.920]	0.121 [0.114, 0.128]
A781	3.143 [0.711, 11.880]	6.374 [5.830, 6.770]	0.111 [0.103, 0.118]
A1763	1.222 [0.480, 2.509]	1.885 [1.686, 2.039]	0.139 [0.135, 0.143]
A2744	11.050 [7.995, 14.070]	2.637 [2.490, 2.760]	0.101 [0.098, 0.103]
A209	0.5185 [0.136, 1.465]	1.321 [1.150, 1.460]	0.176 [0.170, 0.181]
A2163	14.850 [13.770, 16.120]	5.970 [5.890, 6.020]	0.116 [0.115, 0.118]
RXCJ2003.5-2323	4.602 [2.507, 9.255]	1.824 [1.440, 1.970]	0.062 [0.059, 0.064]
A520	5.259 [4.779, 5.588]	10.050 [10.030, 10.110]	0.0976 [0.0971, 0.0983]
A773	1.445 [0.659, 2.705]	2.403 [2.220, 2.530]	0.184 [0.179, 0.188]
A1758a	2.515 [1.492, 3.697]	8.217 [8.070, 8.320]	0.109 [0.106, 0.111]
A1351	3.506 [1.900, 7.398]	4.272 [3.872, 4.527]	0.083 [0.079, 0.088]
A2219	1.681 [1.228, 2.068]	2.127 [2.070, 2.190]	0.134 [0.133, 0.136]
A521	5.090 [2.981, 7.771]	2.204 [2.030, 2.470]	0.108 [0.104, 0.111]
A697	1.668 [0.790, 3.919]	0.731 [0.580, 0.890]	0.153 [0.149, 0.157]
A1300	6.847 [4.079, 12.880]	4.442 [4.230, 4.640]	0.191 [0.185, 0.197]
RXC J1514.9-1523	1.411 [0.491, 2.995]	1.301 [1.063, 1.429]	0.064 [0.062, 0.066]
A1682	15.320 [8.342, 24.490]	2.054 [1.820, 2.390]	0.126 [0.119, 0.132]
A1443	12.890 [6.644, 21.020]	3.530 [3.138, 3.817]	0.109 [0.101, 0.115]
Z5247	3.061 [0.744, 8.739]	3.362 [2.890, 3.667]	0.158 [0.138, 0.173]
A2552	0.222 [0.106, 1.383]	0.639 [0.523, 0.824]	0.218 [0.212, 0.224]
RXC J0510.7-0801	2.171 [0.885, 4.356]	2.346 [2.140, 2.590]	0.134 [0.129, 0.138]
A402	1.350 [0.793, 3.169]	1.249 [1.109, 1.399]	0.323 [0.315, 0.331]
A2895	4.851 [2.929, 7.732]	4.271 [4.020, 4.440]	0.161 [0.155, 0.167]
A2813	1.230 [0.396, 3.239]	0.311 [0.300, 0.550]	0.172 [0.168, 0.176]
PSZ1G139.61+24	0.194 [0.074, 0.965]	1.348 [1.175, 1.526]	0.362 [0.358, 0.369]
A2355	7.495 [4.403, 12.331]	4.879 [4.458, 5.066]	0.075 [0.071, 0.080]
A1733	0.299 [0.629, 7.244]	4.219 [3.738, 4.642]	0.134 [0.121, 0.142]
MACS J2135-010	4.073 [2.203, 10.711]	1.188 [0.917, 1.445]	0.139 [0.133, 0.144]